Available online at www.sciencedirect.com

ScienceDirect

Mendeleev Commun., 2019, **29**, 672–674

Mendeleev Communications

Visible light responsive Ni-doped micro/nanostructured Bi_2O_3 microspheres for photocatalytic denitrification of fuel oil

Qingming Meng* and Zhiquan Yin

College of Chemistry and Chemical Engineering, Bohai University, Jinzhou 121013, P. R. China. E-mail: qingmingmeng@163.com

DOI: 10.1016/j.mencom.2019.11.023

The title microspheres were synthesized by a parallel flow precipitation process using $Bi(NO_3)_3·5H_2O$, $Ni(NO_3)_2·6H_2O$ and $(NH_4)_2CO_3$. The crystalline phase of Ni-doped Bi_2O_3 gradually changed from α-Bi_2O_3 to β-Bi_2O_3, and its morphology varied from irregular chips to the self-assembly microspheres and microflowers when Ni was introduced into Bi_2O_3. The microspheres doped with 3 at% Ni exhibited much higher photocatalytic activity in the photodegradation of pyridine than that of pure Bi_2O_3.

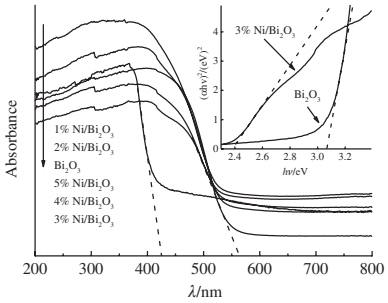

Bismuth oxide, a semiconductor with a large energy band gap and remarkable photoconductivity, is of interest due to its applications in environmental pollution control and energy conversion.[1] Usually, it has four crystalline phases: monoclinic (α-Bi_2O_3), tetragonal (β-Bi_2O_3), body-centered cubic (γ-Bi_2O_3) and face-centered (δ-Bi_2O_3). Among them, low-temperature stable α-Bi_2O_3 and high-temperature metastable β-Bi_2O_3 have been sufficiently exploited due to their outstanding optical properties and high ionic conductivity.[2,3] As a promising photocatalyst, β-Bi_2O_3 exhibited higher photocatalytic efficiency than α-Bi_2O_3 because of lower band gap energy and higher optic absorbance ability in the wider visible light range.[4] In a few reports on metastable β-Bi_2O_3, it was acquired by heating transform of α-Bi_2O_3.[5] To promote the photocatalytic activity of Bi_2O_3 under sunlight irradiation, metal ions (such as Cu,[6] Er[7] and Sr[8]) were introduced into Bi_2O_3. The metal doping introduced an impurity energy level above the valence band of Bi_2O_3, and the conduction band was negative[9,10] to hamper the fast recombination of photoexcited electrons and holes and to enhance photocatalytic performance. Nickel is a good candidate as a dopant in Bi_2O_3. The ionic radii of Ni^{2+} and Bi^{3+} are 0.069 and 0.103 nm, respectively; thus, it is theoretically probable for Ni^{2+} to replace Bi^{3+} in the Bi_2O_3 lattice. Moreover, Ni-doped Bi_2O_3 fabricated by Malathy *et al.*[11] could be applied to efficient sunlight-driven photocatalysis.

In this work, we developed a parallel flow precipitation process for the preparation of self-assembly Ni-doped micro/nanostructured β-Bi_2O_3 microspheres† and studied the effect of Ni doping on the morphology and structure of Bi_2O_3 and the photocatalytic denitrification of fuel oil (using a solution of pyridine in light petroleum to simulate fuel oil).‡

The crystalline phases of Bi_2O_3 and Ni-doped Bi_2O_3 were characterized by XRD patterns [Figure 1(*a*)].§ The main diffraction peaks at 25.80, 26.94, 27.45, 28.05, 32.58, 46.37, 52.44, 53.06 and 54.83° were detected in the Bi_2O_3 sample, which can be assigned to monoclinic α-Bi_2O_3 (JCPDS no. 71-0465). For the 1% Ni/Bi_2O_3 sample, the diffraction peaks of α-Bi_2O_3 phase gradually disappeared, but some main peaks at 25.77, 27.98, 31.73, 32.73, 46.21, 46.89, 54.25, 55.49 and 57.77° appeared, which were indexed to tetragonal β-Bi_2O_3 (JCPDS no. 49-1762). When the molar Ni/Bi ratio was ⩾2%, α-Bi_2O_3 was completely transformed into β-Bi_2O_3. This was due to the fact that Ni doping altered the driving force in the formation of crystal cell and the dominant growth direction.[12] At the Ni/Bi molar ratio of 3%, the FWHM of the 3% Ni/Bi_2O_3 sample was enhanced, illustrating that its average crystal size decreased. According to the Scherrer equation, the crystal sizes of sole Bi_2O_3 and Ni-doped Bi_2O_3 were calculated separately using the (-121)

† Different amounts of $Ni(NO_3)_2·6H_2O$ and 9.71 g of $Bi(NO_3)_3·5H_2O$ were dissolved in 25 ml of deionized water and labelled O. With two constant flow pumps, solution O and $(NH_4)_2CO_3$ (0.75 mol dm^{-3}) were simultaneously infused into the identical reactor under incessant and vigorous stirring. The pH of reaction system was 7.2. After being washed (5x) with deionized water, the precipitate was dried by spray drying to form a homogeneous powder. Then, the above mixture was sintered at 400 °C for 1.5 h with a heating rate of 2 K min^{-1} and allowed to cool naturally. The photocatalysts Bi_2O_3, 1% Ni/Bi_2O_3, 2% Ni/Bi_2O_3, 3% Ni/Bi_2O_3, 4% Ni/Bi_2O_3 and 5% Ni/Bi_2O_3 doped with 0, 1, 2, 3, 4 and 5 at% Ni, respectively, were synthesized.

‡ A 250 ml quartz beaker with a cooling and oxygen supply device was applied as the reactor. A 20 mg Ni-doped Bi_2O_3 photocatalyst sample was scattered in 100 ml of 100 μg g^{-1} pyridine light petroleum solution. Before irradiation, the suspension was stirred in the dark for 30 min to establish adsorption–desorption equilibrium. Then, the suspension was irradiated under a 500 W Xenon lamp ($\lambda > 420$ nm) with a cut-off filter, which was positioned 15 cm above pyridine light petroleum solution. At regular intervals, a 2 ml of suspension was sampled, centrifuged and measured at 251 nm by UV-5200 spectrophotometer. The denitrification efficiency (N) was calculated as $N = (N_0 - N_B)/N_0 \times 100\%$ (N_0 and N_B are the absorbance of pyridine solution in light petroleum before and after photodegradation, respectively).

§ The crystalline phases of the as-prepared samples were determined on a D/max2200VPC X-ray diffractometer with Cu-Kα radiation (λ = = 1.54056 Å). The morphology and EDX analysis were carried out on a Hitachi S-4800 field emission scanning electron microscope. The UV-visible diffuse reflectance spectra were recorded on a Shimadzu UV-2550 spectrometer.

© 2019 Mendeleev Communications. Published by ELSEVIER B.V. on behalf of the N. D. Zelinsky Institute of Organic Chemistry of the Russian Academy of Sciences.

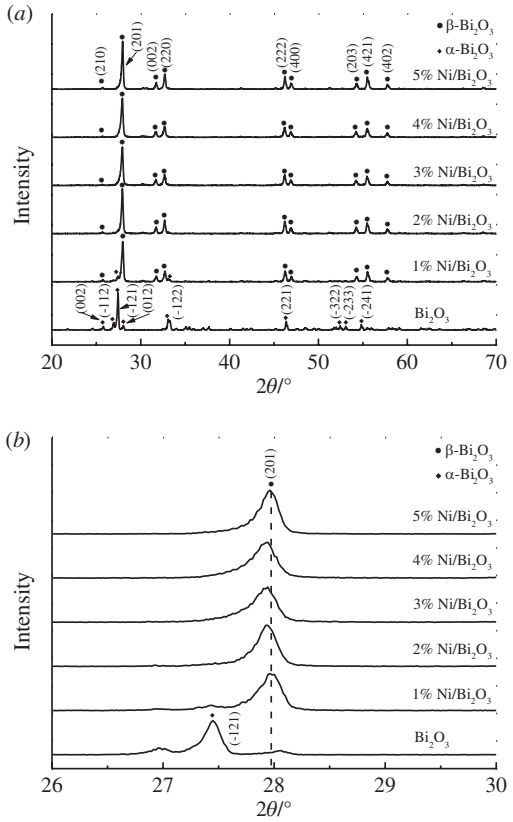

Figure 1 (*a*) XRD patterns of Bi_2O_3 and Ni-doped Bi_2O_3 and (*b*) a comparison of (201) peaks from XRD patterns.

and (201) peaks. The crystal sizes of Bi_2O_3, 1% Ni/Bi_2O_3, 2% Ni/Bi_2O_3, 3% Ni/Bi_2O_3, 4% Ni/Bi_2O_3 and 5% Ni/Bi_2O_3 were 53.5, 39.1, 35.7, 32.4, 32.8 and 41.8 nm, respectively. Ni-doped Bi_2O_3 revealed a slight transformation towards lower values of 2θ [Figure 1(*b*)]. This phenomenon illustrates that the transformation can be contributed *via* Ni ions injected into Bi_2O_3, which may have taken possession of the substitutional cationic sites. Note that there was no transformation of the (201) peak for the 5% Ni/Bi_2O_3 sample. This observation can explain the fact that the section of Ni ions injected into the Bi_2O_3 lattice does not proceed in proportion to the doping content, that is to say, relatively low content of Ni ions is prone to substitute Bi ions. Additionally, the peak of Ni was not observed, suggesting that doping at a certain ratio introduced Ni into the Bi_2O_3 lattice and formed a solid solution.

The morphologies of Bi_2O_3 and Ni-doped Bi_2O_3 are shown in Figure 2.§ The particles of undoped Bi_2O_3 [Figure 2(*a*)] were irregular chips with unsmoothed surface, non-uniform dispersion and obvious aggregation. With increasing the amount of Ni dopant, spherical and flower-shaped products [Figures 2(*b*) and 2(*c*)] were gradually formed. The perfect self-assembly of Bi_2O_3 microspheres was obtained at Ni/Bi of 3% [Figure 2(*d*)]. On further increasing the amount of Ni, the images of 4% Ni/Bi_2O_3 and 5% Ni/Bi_2O_3 [Figures 2(*e*) and 2(*f*)] displayed flower-like structures. More-over, the EDX mappings of Bi, O and Ni elements confirmed their presence in the 3% Ni/Bi_2O_3 sample [Figure 2(*g*)], which is consistent with the XRD results.

The optical absorption performance of a photocatalyst is generally considered as a crucial ingredient in determining its photocatalytic activity. Figure 3 shows the UV-VIS spectra of the samples.§ A red shift of the absorption edge can be found in Ni-doped Bi_2O_3 samples. The absorption edge (570 nm) of 3% Ni/Bi_2O_3 red shifted obviously compared with that of the Bi_2O_3 (425 nm), which can improve absorptive capacity of visible light. The band gaps calculated according to the Tauc plot

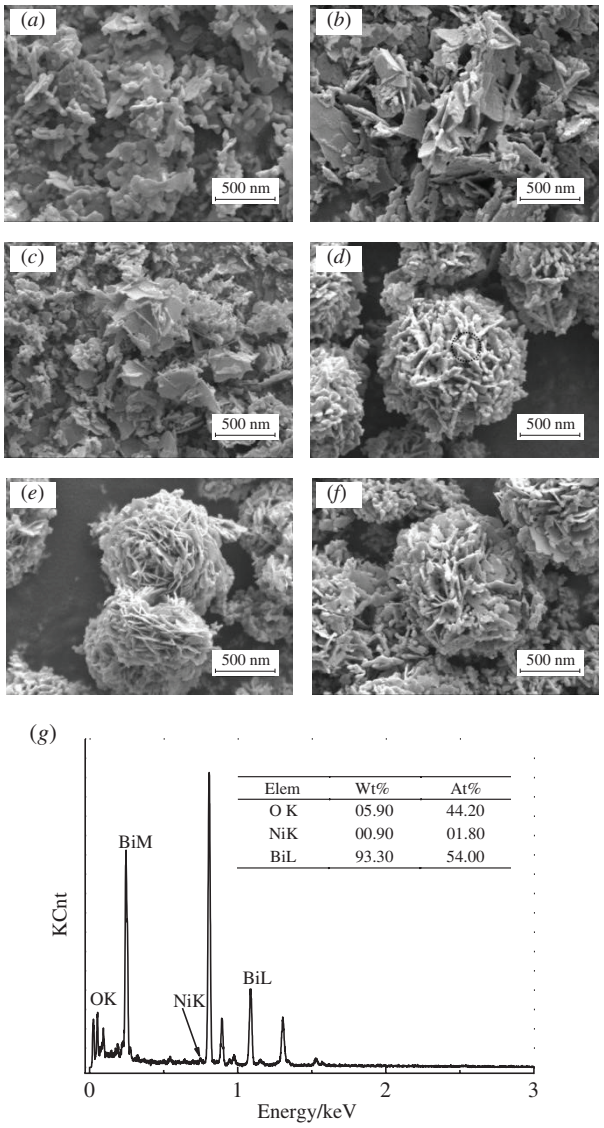

Figure 2 Field emission scanning electron microscopy images of (*a*) Bi_2O_3, (*b*) 1% Ni/Bi_2O_3, (*c*) 2% Ni/Bi_2O_3, (*d*) 3% Ni/Bi_2O_3, (*e*) 4% Ni/Bi_2O_3 and (*f*) 5% Ni/Bi_2O_3; (*g*) the EDX spectrum of 3% Ni/Bi_2O_3.

method[13] were about 2.37 eV for 3% Ni/Bi_2O_3 and 3.06 eV for Bi_2O_3. Thus, the 3% Ni/Bi_2O_3 sample can easily induce more photoelectrons and holes under visible light irradiation.

The degradation of pyridine under visible light in the presence of synthesized photocatalyst was compared with that in the presence of commercial Bi_2O_3 (Sinopharm Chemical

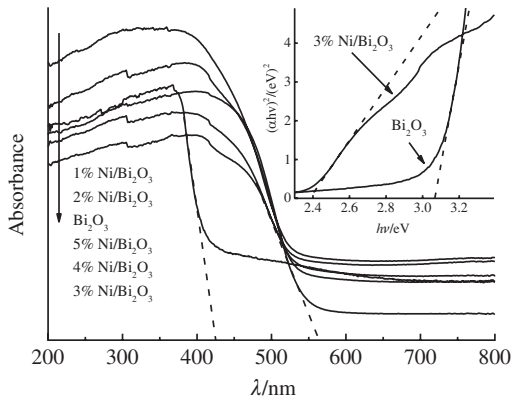

Figure 3 UV-VIS diffuse reflectance spectra of Bi_2O_3 and Ni-doped Bi_2O_3. The inset is bandgap of samples.

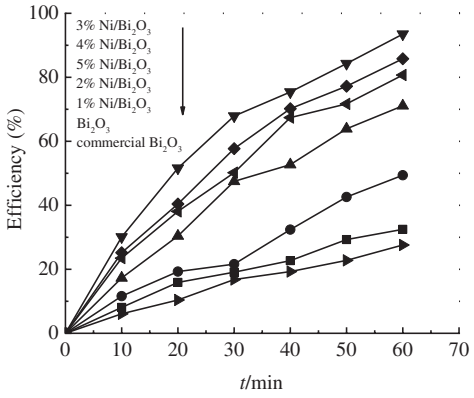

Figure 4 Efficiency of pyridine photodegradation in the presence of the synthesized samples and commercial Bi_2O_3.

Reagent, China) (Figure 4). All the synthesized photocatalysts exhibited better photocatalytic activity as compared with that of commercial Bi_2O_3. The visible-light-induced photocatalytic activity of Ni-doped Bi_2O_3 was much higher than that of pure Bi_2O_3. The best performance was observed for the 3% Ni/Bi_2O_3 sample; after visible light irradiation for 60 min, it was nearly three times as high as that of Bi_2O_3. Doping of Ni into Bi_2O_3 lattice can introduce novel electronic states in Bi_2O_3 to constitute an additional interband site.[14] The electron trapping by this interband site resulted in the forceful prevention of photoexcited electron–hole (e^-–h^+) recombination; hence, effective e^-–h^+ separation was obtained on the photocatalyst surface. As a result, Ni doping increased the number of photoexcited e^- and h^+ to participate in the photocatalytic reaction, which brought about the high photocatalytic activity.

Thus, the result of photodegradation confirms that 3% Ni/Bi_2O_3 microspheres exhibited a mostly outstanding photocatalytic property. The notably high photocatalytic activity stems from the crystalline phase transitions, the special morphology, the broad absorption of excitation light source and the forceful prevention of photoexcited e^-–h^+ recombination.

This work was supported by the Doctoral Scientific Research Foundation of Bohai University (0517bs029).

References

1 S. Iyyapushpam, S. T. Nishanthi and D. P. Padiyan, *J. Phys. Chem. Solids*, 2015, **81**, 74.
2 J. Hou, C. Yang, Z. Wang, W. Zhou, S. Jiao and H. Zhu, *Appl. Catal., B*, 2013, **142**–**143**, 504.
3 K. Valencia G., A. López, A. Hernández-Gordillo, R. Zanella and S. E. Rodil, *Ceram. Int*., 2018, **44**, 22329.
4 M. Jalalah, M. Faisal, H. Bouzid, J. Park, S. A. Al-Sayari and A. A. Ismail, *J. Ind. Eng. Chem. (Amsterdam, Neth.)*, 2015, **30**, 183.
5 Y. Qiu, M. Yang, H. Fan, Y. Zuo, Y. Shao, Y. Xu, X. Yang and S. Yang, *Mater. Lett*., 2011, **65** , 780.
6 W. Qin, J. Qi and X. Wu, *Vacuum*, 2014, **107**, 204.
7 H. Liu, M. Luo, J. Hu, T. Zhou, R. Chen and J. Lia, *Appl. Catal., B*, 2013, **140**–**141**, 141.
8 M. Faisal, A. A. Ibrahim, H. Bouzid, S. A. Al-Sayari, M. S. Al-Assiri and A. A. Ismail, *J. Mol. Catal. A: Chem.*, 2014, **387**, 69.
9 J. Liang, G. Zhu, P. Liu, X. Luo, C. Tan, L. Jin and J. Zhou, *Superlattices Microstruct*., 2014, **72**, 272.
10 H. Sudrajat, *Superlattices Microstruct*., 2017, **109**, 229.
11 P. Malathy, K. Vignesh, M. Rajarajan and A. Suganthi, *Ceram. Int*., 2014, **40**, 101.
12 S. Xue, H. He, Q. Fan, C. Yu, K. Yang, W. Huang, Y. Zhou and Y. Xie, *J. Environ. Sci*., 2017, **60**, 70.
13 C. Chang, H.-C. Yang, N. Gao and S.-Y. Lu, *J. Alloys Compd*., 2018, **738**, 138.
14 Y. Huang, J. Qin, C. Hu, X. Liu, D. Wei and H. Seo, *Appl. Surf. Sci*., 2019, **473**, 401.

Received: 23rd May 2019; Com. 19/5932